The Ligand-Binding Loops in the Tunicate C-Type Lectin TC14 Are Rigid[†]

Sébastien F. Poget, Stefan M. V. Freund,* Mark J. Howard,[‡] and Mark Bycroft

MRC Centre for Protein Engineering, Department of Chemistry, University of Cambridge, Lensfield Road, Cambridge CB2 1EW, U.K.

Received November 27, 2000; Revised Manuscript Received April 3, 2001

ABSTRACT: C-Type lectin-like domains are very common components of extracellular proteins in animals. They bind to a variety of ligands, including carbohydrates, proteins, ice, and $CaCO_3$ crystals. Their structure is characterized by long surface loops in the area of the protein usually involved in ligand binding. The C-type lectin TC14 from *Polyandrocarpa misakiensis* specifically binds to D-galactose by coordination of the sugar to a bound calcium atom. We have studied the dynamic properties of TC14 by measuring ^{15}N longitudinal and transverse relaxation rates as well as $\{^1H-^{15}N\}$ heteronuclear NOEs. Relaxation rates and heteronuclear NOE data for holo-TC14 show minimal variations, indicating that there is no substantial difference in rigidity between the elements of regular secondary structure and the extended surface loops. Anisotropic tumbling of the elongated TC14 dimer can account for the main fluctuations in relaxation rates. Loss of the bound calcium does not significantly alter the internal dynamics, suggesting that the stability of the loop region is intrinsic and not dependent on the coordination of the calcium ion. Chemical shift differences between the holo and apo form show that main structural changes occur in the calcium-binding site, but smaller structural changes are propagated throughout the molecule without affecting the overall fold. The disappearance of two resonances for residues following the conserved *cis*-proline 87 (which is located in the calcium-binding site) in the apo form indicates conformational change on an NMR time scale between the *cis* and *trans* configurations of this peptide bond in the absence of calcium. Possible implications of these findings for the ligand binding in C-type lectin-like domains are discussed.

C-Type lectin-like domains (CTLDs)[1] are among the most common modules in extracellular proteins of animals and are usually involved in cell−cell or cell−matrix interactions. They show a very wide diversity of binding specificity based on a common structural scaffold (*1*). Their name is derived from a subset of members of this protein family, the C-type lectin carbohydrate-recognition domains (CRDs). These proteins show weak but specific calcium-dependent binding to carbohydrates (*2*). For many other CTLDs, noncarbohydrate ligands have been discovered, which include proteins and inorganic surfaces such as ice or $CaCO_3$ (*1*). In the complete genome of *Caenorhabditis elegans*, for example, only 10% of all the 183 identified CTLDs seem to be carbohydrate-binding domains (*3*).

From a large number of crystal structures of carbohydrate- as well as non-carbohydrate-binding CTLDs, the common fold of this protein family is well-known. The typical CTLD structure can be roughly divided into two parts. One half of the molecule consists of a long two-stranded β-sheet (or a three-stranded β-sheet in the long form CTLDs) sandwiched by two α-helices, and the other half consists of shorter stretches of β-sheets and a large proportion of nonrepetitive secondary structure. The carbohydrate-binding site of the C-type lectin CRDs is found in this region. A calcium ion is coordinated by residues from two extended surface loops (termed loops 3 and 4) and from a β-strand (β4). Sugar binding occurs indirectly through coordination of the 3- and 4-hydroxyl oxygens of the sugar to this calcium ion and through direct sugar−protein hydrogen bonds as well as through hydrophobic interactions (only in the galactose-specific lectins) (*4*−*7*). So far there are two crystal structures of CTLDs with protein or peptide ligands. In the structure of the Ly49A natural killer cell receptor CTLD in complex with its MHC class I ligand H-2D^d (*8*), the protein is bound at two sites. The first site corresponds to the sugar-binding sites of carbohydrate-binding C-type lectins, whereas the second site is larger and extends over both molecules of the Ly49A dimer. In a very recently determined crystal structure of the CTLD of P-selectin, a sulfated and glycosylated peptide is bound both through the carbohydrate chain (the sugar binding is similar to that in other CTLDs) and through direct peptide−protein hydrophobic and electrostatic contacts involving two sulfated tyrosine residues (*9*).

One striking feature of CTLD structures is the high percentage of nonregular secondary structure, particularly in the ligand recognition site. This allows the presentation of different elements of binding specificity in varying spatial arrangements, enabling different receptor functions to be

[†] This work was supported by a Roche Research Foundation scholarship to S.F.P. and the Herchel Smith Endowment (S.F.P.).

* To whom correspondence should be addressed. Phone: +44-1223-336 392. Fax: +44-1223-336 445. E-mail: smvf100@cam.ac.uk.

[‡] Present address: Cardiff Laboratories, Amersham Pharmacia Biotech Ltd., Forest Farm, Whitchurch Cardiff, Wales CF14 7YT, U.K.

[1] Abbreviations: CTLD, C-type lectin-like domain; CRD, carbohydrate-recognition domain; MBP, mannose-binding protein; NMR, nuclear magnetic resonance; NOE, nuclear Overhauser effect; TC14, *Polyandrocarpa* lectin; HSQC, heteronuclear single-quantum coherence; CPMG, Carr−Purcell−Meiboom−Gill sequence; FID, free induction decay; $\Delta\delta$, chemical shift difference; rmsd, root-mean-square deviation.

10.1021/bi002698z CCC: $20.00
Published on Web 08/22/2001

performed by proteins sharing the same fold. As the loops have a defined function in the protein and do not merely connect areas of regular secondary structure, the following question arises: Are they flexible parts of the protein that only acquire a defined structure on binding of the ligand, or do they form rigid structure elements and thus display a binding site with a defined geometry?

Heteronuclear relaxation studies are a well-established tool for studying dynamic properties of proteins in solution. They are considered to truly reflect the overall as well as internal mobility of a protein in a near-physiological environment. Here, we have used NMR relaxation techniques to address the question of the mobility of loop regions in CTLDs. ^{15}N relaxation experiments not only probe the mobility of backbone NH vectors on a nanosecond to picosecond time scale but also provide valuable insight into conformational exchange processes on a slower millisecond to microsecond time scale. In this study, the specifically D-galactose binding *Polyandrocarpa* lectin (TC14) was used (*10*). This C-type lectin is involved in sorting undifferentiated hemoblasts and pluripotent stem cells in the bud vesicle of the ascidian *Polyandrocarpa misakiensis* during asexual reproduction (*11*). We have recently determined the crystal structure of TC14 complexed with D-galactose and found that TC14 occurs as a dimer in solution and has a single calcium-binding site, which is involved in D-galactose binding (*7*). Here we present the backbone dynamic properties of holo- and apo-TC14.

EXPERIMENTAL PROCEDURES

Protein Expression and Purification. TC14 was expressed in *Escherichia coli* and purified as described elsewhere (*7*). Uniformly ^{15}N singly labeled and ^{13}C/^{15}N doubly labeled TC14 was produced by growing cells in M9 minimal medium containing $^{15}NH_4Cl$ as the sole nitrogen source and [$^{13}C_6$]-glucose as the sole carbon source for the doubly labeled protein.

NMR Sample Preparation. For the preparation of holo-TC14 samples, uniformly ^{15}N- and ^{13}C/^{15}N-labeled TC14 was first dialyzed into 20 mM MOPS (pH 7.0), 20 mM $CaCl_2$, and 50 mM NaCl and then three times into a 100-fold excess of H_2O. Samples were adjusted to pH 7.0 with small aliquots of HCl and NaOH and concentrated to 0.8−1 mM in an Amicon centriprep 10 concentrator. Apo-TC14 samples were prepared by dialyzing uniformly ^{15}N- and^{13}C/^{15}N-labeled TC14 into 20 mM EDTA (pH 7.0) and concentrating to 0.8−1 mM. Immediately before the measurement of NMR data, any precipitate was removed by spinning the samples at 16000*g* for 5 min.

NMR Spectroscopy. All spectra were recorded on Bruker AMX 500 and DRX 600 NMR spectrometers equipped with triple-resonance probes and *z*-axis gradients at 310 K (apart from holo-TC14 T_1 and T_2 experiments which were also carried out at 298 K). ^{1}H/^{15}N HSQC spectra were recorded with 256 complex points in the indirect dimension. Water suppression was achieved by water flipback pulses (*12*) or using the WATERGATE scheme (*13*). Cross-peaks in the HSQC spectra of TC14 at 310 K were assigned on the basis of the assignments of TC14 at 328 K (*14*) and confirmed by a combination of HNCA (*15*), HNCACB (*16*), and CBCA-(CO)NH (*17*) triple-resonance experiments. For apo-TC14, ambiguities in the assignment could mostly be resolved through sequential correlation of the carbonyl carbon resonance shifts using a combination of HNCO (*15*) and HN-(CA)CO (*18*) experiments. Acquired NMR data were converted to FELIX format using the program ux2flx and processed with FELIX version 2.30 (Biosym Technologies). FIDs were multiplied with an exponential window function before Fourier transformation. Proton chemical shifts were referenced on the basis of the water frequency for protons and indirectly for heteronuclei (*19*).

^{15}N T_1, T_2, and {^{1}H−^{15}N} NOE experiments (*20*) were recorded at a ^{15}N frequency of 50.13 MHz on a Bruker AMX 500 spectrometer. T_1 relaxation delays were set to 40, 80, 120, 200, 280, 360, 480, 600, 720, 840, and 1000 ms for holo-TC14 at 310 K and to 40, 80, 120, 200, 280, 360, 440, 520, 600, 720, 880, and 1000 ms for apo-TC14 and holo-TC14 at 298 K. T_2 experiments featured a CPMG pulse train with a spin-echo delay, 2τ, of 0.9 ms. T_2 relaxation delays were set to 7, 28, 42, 56, 70, 84, 98, 112, 126, 140, 168, and 196 ms for holo-TC14 at 310 K and to 7, 14, 28, 42, 56, 70, 84, 98, 112, 126, 140, 168, and 196 ms for apo-TC14 and holo-TC14 at 298 K. Overall relaxation delays were set to 3 s in all experiments. Peak heights were fitted to a monoexponential decay function using Kaleidagraph 3.0 (Abelbeck Software). The standard errors from the Levenberg−Marquardt fitting routine were taken as the uncertainties in the obtained R_1 and R_2 values, and were typically in the range of 2−4% for apo-TC14, 4−6% for holo-TC14 at 310 K, and 5−15% for holo-TC14 at 298 K. {^{1}H−^{15}N} NOEs were determined from spectra obtained with and without presaturation of amide proton resonances. Presaturation was achieved by applying 120° decoupling pulses in 5 ms intervals with a field strength of 25 kHz for 3 s. Reference spectra were obtained by replacing the presaturation sequence with a simple delay of the same length. For both experiments, the overall recycle delay was set to 5 s. The NOE enhancement η was calculated according to the formula

$$\eta = \frac{I' - I_0}{I_0}$$

where I' and I_0 are the peak intensities in the spectrum with and without presaturation, respectively. Two sets of interleaved NOE and control experiments were added to obtain the intensities used in the calculation.

RESULTS

NMR Resonance Assignment and Chemical Shift Analysis. We previously published complete assignments of holo-TC14 at 328 K (*14*). At 310 K, however, HSQC spectra of TC14 showed an increased level of line broadening and regions of overlapping peaks in the center of the spectrum so that only 114 of 120 non-proline residues were assigned in the HSQC spectrum of holo-TC14 (111 residues for apo-TC14). The most striking difference between the HSQC spectra of holo- and apo-TC14 is in the extent of line broadening. At the same temperature and concentration, the apo form yields significantly sharper signals (Figure 1). Apart from this, the two forms have very similar spectra, which shows that there are no global structural changes upon calcium binding in

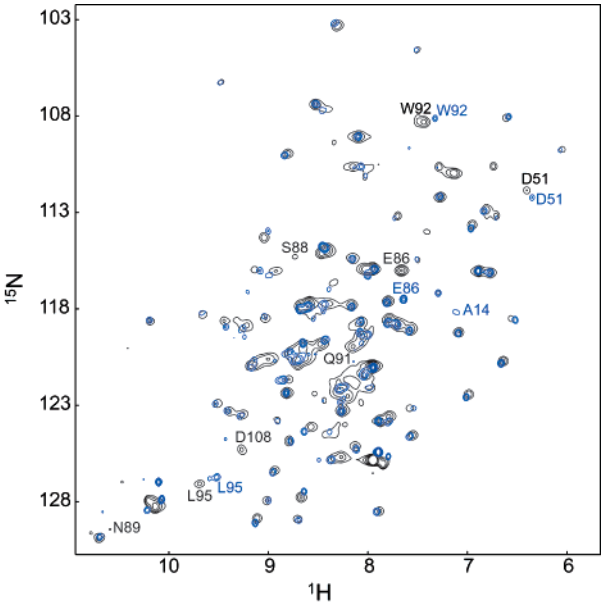

FIGURE 1: Overlay of HSQC spectra of holo-TC14 (black) and apo-TC14 (blue) at 310 K. Peaks missing in either of the two forms or significantly shifted peaks are labeled in the corresponding color.

TC14. Most of the chemical shift differences ($\Delta\delta$) between holo- and apo-TC14 are found in the calcium-binding region. Smaller $\Delta\delta$s occur between the end of strand β1 and the beginning of helix α1, before and after helix α2, and in loop 1 (Figure 2).

The most significant $\Delta\delta$s involve two residues directly involved in calcium binding. Glu86 exhibits a $\Delta\delta$ of −1.51 ppm in its amide nitrogen chemical shift, whereas Asp107 exhibits a $\Delta\delta\{C\alpha - C\beta\}$ of 1.11 ppm. The amide $\Delta\delta$ in Glu86 indicates a major change in the chemical environment, whereas the $\Delta\delta\{C\alpha - C\beta\}$ in Asp107 is indicative of a difference in secondary structure. In β-sheets, the average Cα chemical shifts are lower and the average Cβ shifts higher than in random coil. Asp107 exhibits an increased Cα and a decreased Cβ chemical shift in apo-TC14, which means that this residue, which is part of β-strand β4, has reduced secondary structure characteristics in the absence of calcium. The local destabilization of strand β4 in the absence of bound calcium can be explained by the particular structure of the following residue in the strand, Asp108. This residue binds to calcium through both its main chain carbonyl oxygen and its side chain carboxyl oxygen, and therefore, the absence of calcium leads to a less restricted conformation of this residue, loosening β-strand b4. Resonances for Asp108 are present in the spectra of holo-TC14 but missing in apo-TC14, which is most likely caused by line broadening due to conformational exchange. This further supports the idea that Asp108 accesses multiple conformations in the calcium-free form. Another three residues in the immediate vicinity of the calcium-binding site (Ser88, Asn89, and Val109) also exhibit the same behavior, indicating an increase in conformational flexibility in these residues upon loss of calcium.

In addition to differences in the calcium-binding site, chemical shift perturbations in other regions of TC14 indicate that small structural differences between the two states exist throughout the molecule. This indicates that structural changes at the calcium-binding site can be propagated throughout the molecule and cause minor conformational

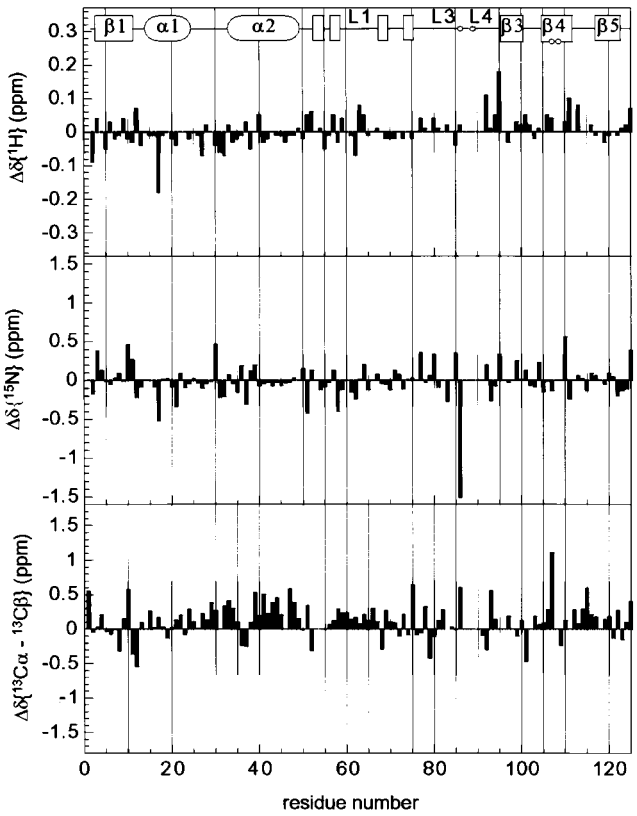

FIGURE 2: ^{1}H, ^{15}N, and ^{13}C chemical shift differences between apo- and holo-TC14. A diagram at the top of the figure indicates the elements of secondary structure with square boxes for β-strands and ovals for α-helices. The secondary structure elements are labeled (with the exception of strands β2, β', and β'', loop 2, and strand β''', which correspond in this order to the unlabeled secondary structure elements). The calcium-binding residues are represented by small spheres. The gray shading represents an area of ±1.5 standard deviations.

changes at remote residues without changing the overall structure.

Backbone Dynamics. The backbone dynamics of TC14 at 310 K in the presence and absence of calcium were analyzed by measurement of longitudinal (R_1) and transverse (R_2) relaxation rates as well as by $\{^1H-^{15}N\}$ heteronuclear NOEs. The resulting relaxation rates and the NOE enhancements are summarized in Figure 3. The average R_1 values are lower in the calcium-bound protein (average of 1.05 ± 0.05 s^{-1}) than in the calcium-free protein (average of 1.28 ± 0.03 s^{-1}), whereas the average R_2 values are higher in the calcium-bound form (16.2 ± 0.63 s^{-1}) than in the calcium-free form (12.2 ± 0.20 s^{-1}). Using the model-free formalism of Lipari and Szabo (*21*, *22*), an estimate for the rotational correlation time τ_c was obtained on the basis of these average R_2/R_1 values for both holo- and apo-TC14 (14.6 and 11.3 ns, respectively).

To interpret this difference in overall correlation time and to allow comparison with other proteins, longitudinal and transverse relaxation experiments were repeated for holo-TC14 at 298 K. The obtained average relaxation rates were 0.91 ± 0.08 s^{-1} for R_1 and 18.2 ± 3.1 s^{-1} for R_2 (the larger errors are due to a further increase in the extent of line broadening at 298 K). From these values, the overall correlation time τ_c can be calculated as 16.9 ns, which is high for a 28 kDa dimer. Analytical ultracentrifugation of holo-TC14 has shown that the molecule is present as a dimer

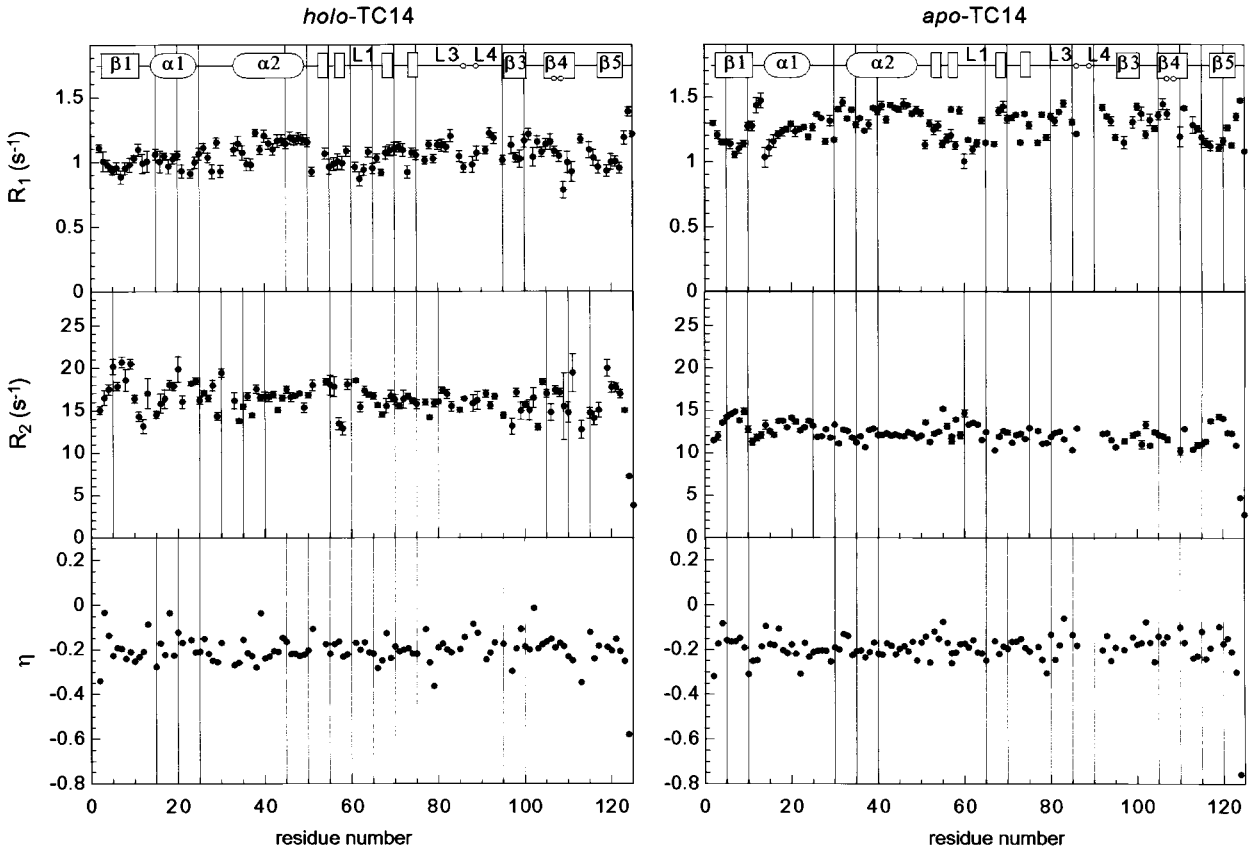

FIGURE 3: R_1, R_2, and $\{^1H-^{15}N\}$ NOE data for holo- and apo-TC14. For the R_1 and R_2 values, error bars are shown for each residue. The secondary structure elements are shown as they are in Figure 2.

with ~5% of higher-order aggregates in solution (*7*). As the concentrations used for the NMR relaxation experiments were significantly higher than in the analytical ultracentrifugation, an even larger fraction of higher-order aggregates is expected under NMR conditions. The observed increase in the overall correlation time for holo-TC14 would occur if these higher-order aggregates were in an equilibrium with the dimeric form of the protein (with association rates faster than the relaxation rates but slower than the overall correlation time). A similar effect has been observed in HIV-1 Nef (*23*). It is possible that higher-order aggregation is either directly mediated by calcium or facilitated by small structural changes in TC14 upon binding of calcium.

Because of the elongated shape of the TC14 dimer (see Figure 4), anisotropic tumbling has to be considered in the analysis of its relaxation rates. In the original model-free approach, overall tumbling motion is considered to be isotropic. This simple assumption can lead to fictitious contributions to the internal motion if the rotational diffusion tensor is significantly anisotropic. To take into account the anisotropic contributions to the relaxation rates in TC14, we have determined the rotational diffusion tensor based on the crystal structure and the relaxation data using the program TENSOR (*24*). Due to the contributions from higher-order aggregates in the calcium-bound form, only results for the apo form are presented, but qualitatively similar results were obtained for the holo form. The relaxation data for 91 residues (83% of all measured relaxation rates) were included in the calculations (residues showing increased internal mobility or conformational exchange were discarded). On the basis of the experimental data, the best fit was achieved using a fully anisotropic model ($\chi^2 = 52.3$), with a slightly worse fit for a prolate axially symmetric model ($\chi^2 = 54.3$) and a much worse fit for an oblate axially symmetric model ($\chi^2 = 202.1$). Monte Carlo sampling methods were used to estimate the reliability of the different models and to estimate the errors in the proposed diffusion tensor. This revealed that the improvement of the fully anisotropic over the prolate model is not statistically relevant, and that the oblate model has to be rejected. The prolate model resulted in a $D_{\|}/D_{\perp}$ ratio of 1.58 ± 0.04. Figure 5 shows a comparison between the experimental R_2/R_1 values and the theoretical values obtained from the prolate axially symmetric model.

Because of the pronounced anisotropy of the molecule and the contributions of the higher-order aggregates in holo-TC14, a spectral density mapping or model-free analysis of the relaxation rates was not undertaken. Instead, a direct interpretation of the experimental data was attempted. Apart from the offset in the R_1 and R_2 values between holo- and apo-TC14, the overall backbone dynamics of both forms are very similar. After accounting for the effects of anisotropic tumbling, we find the relaxation rates show little variation throughout the molecule. The heteronuclear NOE experiments are an independent probe for internal mobility on a picosecond time scale. They are not influenced by conformational exchange processes and confirm that the internal mobility of residues does not vary significantly throughout the molecule. Furthermore, they show that the fast dynamics are very similar between the calcium-bound and calcium-free forms. It can be concluded that in TC14 the elements of nonregular secondary structure (especially loops 3 and 4) represent regions of defined and rigid structure similar to

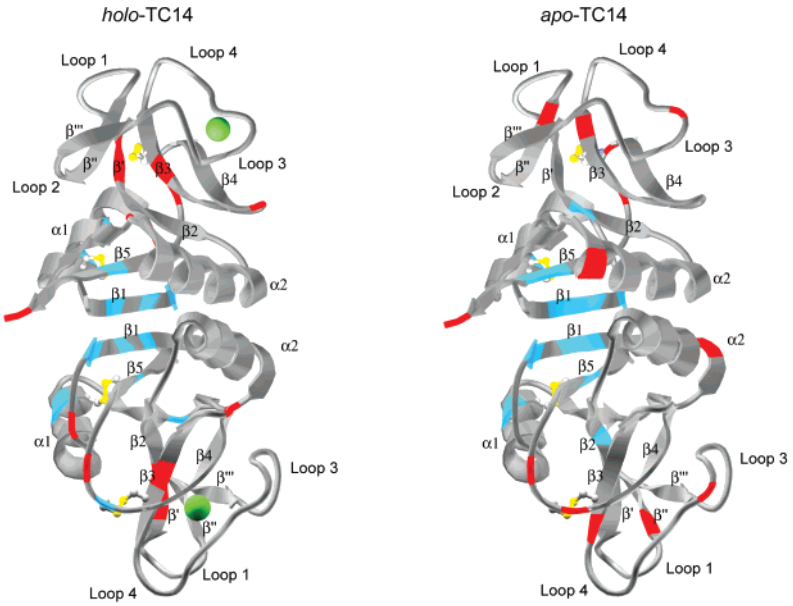

FIGURE 4: Exceptionally high and low R_2 values for holo- and apo-TC14 mapped onto a ribbon diagram of the holo-TC14 dimer. Residues with R_2 values more than 1.5 standard deviations above average (internal motion) are shown in red, and residues with values more than 1.5 standard deviations below average (conformational exchange) are shown in blue. All visible elements of secondary structure are labeled in both copies of the dimer. The calcium atom is shown as a green sphere, and the disulfide bonds are shown in a ball-and-stick representation.

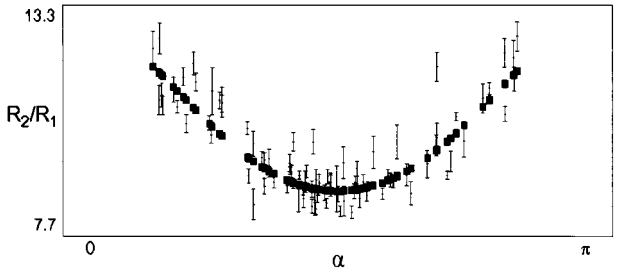

FIGURE 5: Theoretical values of R_2/R_1 calculated from a prolate axially symmetric model with the program TENSOR plotted as black squares against the angle of the NH vector to the principal anisotropic axis and compared to the experimental values shown by their error bars.

regular secondary structure elements. Furthermore, the absence of calcium in the binding site does not seem to affect the overall ^{15}N NMR dynamics of the loop region (with the exception of residues Ser88, Asn89, Asp108, and Val109, which could not be observed in apo-TC14).

The only region with clearly increased flexibility is the loop connecting β-strands β4 and β5, which shows both reduced R_2 rates and NOE enhancements in holo-TC14 and to a lesser extent in apo-TC14. The short loop that connects strand β1 with helix α1 also shows reduced R_2 values in holo-TC14 (to a much lesser extent in the apo form), but no effect is visible in the heteronuclear NOE data, which indicates motion on a slower time scale. In addition, there are a few isolated residues that display increased mobility; none of them is present in both holo- and apo-TC14, and only one of them, Asn85 in the apo form, involves a residue from the extended loops 3 and 4 (Figure 4).

A number of residues exhibit above-average R_2 values (Figure 4), which are usually interpreted as representing a conformational exchange slower than the rotational correlation time. In holo-TC14, the increase in R_2 that affects all residues and is caused by the equilibrium aggregation of the protein has to be discounted. Three residues at the dimeric interface (Ile5, Phe7, and Asp9) exhibit additionally increased R_2 values. The amide groups of these residues form intermolecular hydrogen bonds, and therefore, small movements at the dimeric interface lead to this conformational exchange behavior. A similar effect has previously been observed at the dimeric interface of the inhibitor-bound HIV protease (*25*). In apo-TC14, the conformational exchange effect at the dimeric interface is less obvious, but residues Ile5, Leu6, Phe7, and Asp9 also exhibit above-average transverse relaxation rates. Further conformational exchange effects can be observed in a number of residues in the vicinity of a disulfide bridge. They comprise Tyr20, Cys111 (only in the holo form), Cys119, and Glu120 (only in the apo form). In addition, residue Ser30 in holo-TC14 and Val55 in apo-TC14 also exhibit increased R_2 values.

Comparison of NMR Dynamics and Crystallographic B-Factors. As dynamic effects can influence temperature factors in crystal structures, we have compared the results of the NMR backbone dynamics to the temperature factors from the crystal structure of TC14 (PDB entry 1byf). In contrast to the uniform dynamic behavior revealed by NMR, the temperature factors show considerable variation throughout the molecule (Figure 6). Temperature factors reflect the disorder in the crystal and are influenced by several factors. First, they are influenced by the dynamics of the protein in the crystal. These can differ from those in solution due to the constraints of the protein in the crystal lattice. Different conformations caused by slow hinging movements of whole structure elements that cannot be observed on an NMR time scale can be frozen out in the crystal. This could explain the overall increase in temperature factors in the extended loop regions. Also, thermal trembling of the protein in the crystal lattice will have the strongest effect on the edges of the molecule, again affecting the extended loop region the most. In the crystal structure of TC14, some areas of increased temperature factors (residues 35−40, 60−63, 91−94, and 102−104) also exhibit increased rmsd values of 0.3−0.4 Å

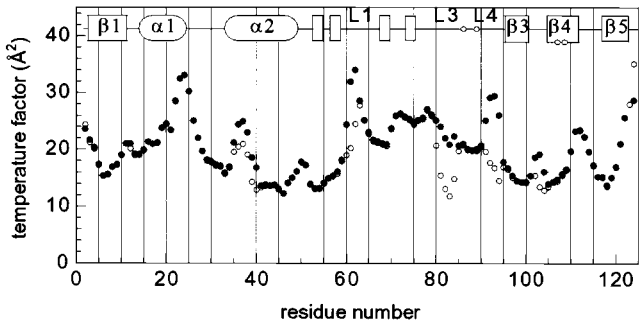

FIGURE 6: Temperature factors of the amide nitrogen atoms in the crystal structure of TC14 plotted vs their residue number. Values from molecule A in the asymmetric unit are shown as black circles, whereas values from molecule B are shown as white circles. The elements of secondary structure are shown as they are in Figure 2.

between equivalent amide nitrogens in the two molecules of the asymmetric unit. Therefore, these higher temperature factors may be related to the noncrystallographic symmetry restraints used in the refinement, especially as in these areas the *B*-factors also differ between the two molecules in the asymmetric unit. In the study of TC14, we have used NMR and crystallography as complementary techniques to obtain a complete picture of structural and dynamic aspects of this protein and therefore a thorough structural basis for understanding its function.

DISCUSSION

Currently, there is growing interest in the relationship between protein dynamics and ligand binding. Studying protein dynamics can provide information about and reveal the location of the conformational changes that are coupled to the function of the protein (*26*). The TC14 sugar-binding site consists of residues from loops 3 and 4 (a surface loop structure 20 amino acids in length) and from β-strand β4. The results of ^{15}N NMR dynamics studies show that holo-TC14 has similar dynamic behavior throughout the molecule. Therefore, the extended surface loop region is rigid, and the carbohydrate-binding site of TC14 is formed by structurally well determined and rigid elements. It is interesting to note that the only region of clearly increased mobility in holo-TC14 is the nonfunctional loop connecting β-strands β4 and β5.

The rigidity of the TC14 binding site is in contrast to the observation that binding site residues often exhibit increased flexibility, particularly in proteins that bind to nucleic acids or to other proteins (*26*). In TC14, sugar specificity is achieved by the positioning of hydrogen-bond donors and acceptors around the 3- and 4-hydroxyl oxygens of the bound galactose and the presence of a tryptophan residue that packs against the apolar side of the pyranose ring. To ensure the correct positioning of these elements in very close space, it appears that the binding site has to be rigid. Protein and DNA binding sites are usually much larger, and residues conferring selectivity are further apart. In this case, even a flexible binding site can ensure the correct positioning of the binding residues. Also, a flexible binding site can form tighter interactions with a large structure by adopting a conformation that would be unfavorable in the free state.

Examination of the structure of TC14 suggested several features that could contribute to the rigidity of loops 3 and 4. Four proline residues (positions 76, 84, 87, and 90) are present in this region. The limited conformational flexibility of these residues together with the presence of an extensive hydrogen-bonding network within the loops stabilizes the internal loop structure. Further stabilization comes from a number of key contacts to other parts of the protein. Hydrogen bonds are linking residues Thr77 and Asn89 to strand β'', residues Leu81 and Ser83 to strand β4, and residue Leu95 to strand β'. Indirect linking of residues Glu86 and Asn89 to strand β4 is achieved through the bound calcium ion. Hydrophobic contacts involve loop residues Trp82 and Pro87, which are part of a highly aromatic hydrophobic core that also includes residues Phe67 (from strand β'') and Leu106 (from strand β4).

In a subgroup of CTLDs, the proline residue equivalent to Pro87 in TC14 is conserved. If all CTLD crystal structures are superimposed, the highly aromatic hydrophobic core that stabilizes the loop region in TC14 is found in all domains where this proline is conserved (among the CTLDs of known three-dimensional structure, Pro87 is conserved in all calcium-binding CTLDs and in lithostathine). The only difference is that Leu106 in TC14 is replaced with a tryptophan in all other proteins. In addition, the backbone hydrogen bonds between residues Leu81 and Ser83 and strand β4 are also conserved in all these proteins. The conservation of loop-stabilizing elements throughout this subgroup of CTLDs suggests that this rigidity found in TC14 could be a general feature in those domains. This statement is especially applicable to the second half of loop 3 and the calcium-binding site, where most of these elements are located. This part of the loop region also shows the smallest variations in structure between all CTLDs. Predictions for the dynamic behavior of loop 4 in other CTLDs are more difficult due to the presence of a secondary calcium-binding site between loops 1 and 4 in many other CTLDs.

The overall backbone dynamics of TC14 are not affected by the binding of calcium. However, line broadening in the immediate vicinity of the binding site indicates conformational exchange for these residues. In all calcium-binding C-type lectins, the conserved proline 87 is preceded by a *cys*-peptide bond. Residues immediately before and after this proline are involved in calcium and sugar binding, and the *cis* conformation is believed to be very important for achieving the correct spatial arrangement of the calcium ligands. In a crystallographic study of apo rat liver mannose-binding protein (MBP-C) (*27*), this peptide bond was found to be present in both *cis* and *trans* conformations. In the HSQC spectrum of the apo form of TC14, the peaks for Ser88 and Asn89 are missing. This might be due to conformational flexibility in this region resulting from *cis*−*trans* isomerization of the peptide bond preceding Pro87.

In summary, we found that the extended loop regions in TC14 are rigid, and this rigidity is inherent and not a consequence of the bound calcium ion. Key elements for achieving the rigidity of the carbohydrate-binding site in TC14 are conserved in other CTLDs. This suggests that the ligand-binding site might be rigid in all C-type lectin domains that contain the conserved proline equivalent to Pro87 in TC14. Given the variety of binding properties of CTLDs, it would be very interesting to compare protein dynamics across the whole family and see if the binding site flexibility really varies in the function of the different types of ligands.

ACKNOWLEDGMENT

We thank Alan Fersht for providing support and facilities and Roger Williams for helpful discussions.

REFERENCES

1. Drickamer, K. (1999) *Curr. Opin. Struct. Biol. 9*, 585−590.
2. Drickamer, K. (1988) *J. Biol. Chem. 263*, 9557−9560.
3. The *C. elegans* Sequencing Consortium (1998) *Science 282*, 2012−2018.
4. Weis, W. I., Drickamer, K., and Hendrickson, W. A. (1992) *Nature 360*, 127−134.
5. Ng, K. K. S., Drickamer, K., and Weis, W. I. (1996) *J. Biol. Chem. 271*, 663−674.
6. Kolatkar, A. R., and Weis, W. I. (1996) *J. Biol. Chem. 271*, 6679−6685.
7. Poget, S. F., Legge, G. B., Proctor, M. R., Butler, P. J., Bycroft, M., and Williams, R. L. (1999) *J. Mol. Biol. 290*, 867−879.
8. Tormo, J., Natarajan, K., Margulies, D. H., and Marluzza, R. A. (1999) *Nature 402*, 623−631.
9. Somers, W. S., Tang, J., Shaw, G. D., and Camphausen, R. T. (2000) *Cell 103*, 467−479.
10. Suzuki, T., Takagi, T., Furukohri, T., Kawamura, K., and Nakauchi, M. (1990) *J. Biol. Chem. 265*, 1274−1281.
11. Kawamura, K., Fujiwara, S., and Sugino, Y. M. (1991) *Development 113*, 995−1005.
12. Grzesiek, S., and Bax, A. (1993) *J. Am. Chem. Soc. 115*, 12593−12594.
13. Piotto, M., Saudek, V., and Sklenar, V. (1992) *J. Biomol. NMR 2*, 661−665.
14. Legge, G. B., Poget, S. F., Proctor, M. R., Freund, S. M. V., and Bycroft, M. (2000) *J. Biomol. NMR 18*, 283−284.
15. Grzesiek, S., and Bax, A. (1992) *J. Magn. Reson. 96*, 432−440.
16. Wittekind, M., and Mueller, L. (1993) *J. Magn. Reson., Ser. B 101*, 201−205.
17. Grzesiek, S., and Bax, A. (1992) *J. Am. Chem. Soc. 114*, 6291−6293.
18. Clubb, R. T., Thanabal, V., and Wagner, G. (1992) *J. Magn. Reson. 97*, 213−217.
19. Wishart, D. S., Bigam, C. G., Yao, J., Abildgaard, F., Dyson, H. J., Oldfield, E., Markley, J. L., and Sykes, B. D. (1995) *J. Biomol. NMR 6*, 135−140.
20. Palmer, A. G., Williams, J., and McDermott, A. (1996) *J. Phys. Chem. 100*, 13293−13310.
21. Lipari, G., and Szabo, A. (1982) *J. Am. Chem. Soc. 104*, 4546−4559.
22. Lipari, G., and Szabo, A. (1982) *J. Am. Chem. Soc. 104*, 4559−4570.
23. Grzesiek, S., Bax, A., Hu, J. S., Kaufman, J., Palmer, I., Stahl, S. J., Tjandra, N., and Wingfield, P. T. (1997) *Protein Sci. 6*, 1248−1263.
24. Dosset, P., Hus, J. C., Blackledge, M., and Marion, D. (2000) *J. Biomol. NMR 16*, 23−28.
25. Ishima, R., Freedberg, D. I., Wang, Y. X., Louis, J. M., and Torchia, D. A. (1999) *Struct. Folding Des. 7*, 1047−1055.
26. Ishima, R., and Torchia, D. A. (2000) *Nat. Struct. Biol. 7*, 740−743.
27. Ng, K. K. S., Park-Snyder, S., and Weis, W. I. (1998) *Biochemistry 37*, 17965−17976.
28. Boyington, J. C., Riaz, A. N., Patamawenu, A., Coligan, J. E., Brooks, A. G., and Sun, P. D. (2000) *Immunity 10*, 75−82.

BI002698Z